International Journal of Heat and Mass Transfer 64 (2013) 838–849

Contents lists available at SciVerse ScienceDirect

International Journal of Heat and Mass Transfer

journal homepage: www.elsevier.com/locate/ijhmt

A comprehensive dual-scale wood torrefaction model: Application to the analysis of thermal run-away in industrial heat treatment processes

P. Perré [a,*], R. Rémond [b], I. Turner [c]

[a] Ecole Centrale Paris, LGPM, Grande Voie des Vignes, 92 290 Châtenay-Malabry, France
[b] Université de Lorraine, LERMAB, ENSTIB, 27 rue Philippe Séguin, BP1041, 88051 Epinal cedex 9, France
[c] Queensland University of Technology, School of Mathematical Sciences, GPO Box 2434, Brisbane Q4001, Australia

ARTICLE INFO

Article history:
Received 8 July 2012
Received in revised form 25 March 2013
Accepted 27 March 2013
Available online 4 June 2013

Keywords:
Biomass
Mild pyrolysis
Stack
Board
Simulation
Exothermic reaction
Industrial process

ABSTRACT

A dual-scale model of the torrefaction of wood was developed and used to study industrial configurations. At the local scale, the computational code solves the coupled heat and mass transfer and the thermal degradation mechanisms of the wood components. At the global scale, the two-way coupling between the boards and the stack channels is treated as an integral component of the process. This model is used to investigate the effect of the stack configuration on the heat treatment of the boards. The simulations highlight that the exothermic reactions occurring in each single board can be accumulated along the stack. This phenomenon may result in a dramatic heterogeneity of the process and poses a serious risk of thermal runaway, which is often observed in industrial plants. The model is used to explain how thermal runaway can be lowered by increasing the airflow velocity, the sticker thickness or by gas flow reversal.

© 2013 Elsevier Ltd. All rights reserved.

1. Introduction

In order to prevent attack of wood by fungi or insects, several chemical substances are commonly used. However many of these are hazardous to the environment. The heat treatment of wood under inert atmosphere at temperature levels ranging from 200 °C to 300 °C (mild pyrolysis) is an alternative to the use of chemicals, as it increases the dimensional stability and durability of wood. Due to a thermal degradation of the cell wall constituents, mild pyrolysis significantly changes the material properties, which results in better durability and stability than natural wood [1–4]. However, one has to keep in mind that this is to the detriment of decreased mechanical strength, density and surface roughness [5,6]. In spite of these drawbacks, heat-treated solid wood has become popular and several production plants now exist throughout Europe [7]. These industrial plants must overcome serious problems such as thermal runaway and internal checking to obtain a relevant and homogeneous final product quality. There are several explanations for these phenomena, such as the huge variability of biological products and the dispersion of the initial moisture content and particle shape. However, the dual spatial coupling (within boards and within the stack) in the presence of exothermic reactions is likely to be the main source of problems.

Furthermore, the growing interest in biomass as a source of renewable energy gives rise to a crucial demand in biomass preconditioning. For example, torrefaction is a pretreatment required in the multistep process from biomass to liquid (BtL), which includes a gasification followed by a Fisher-Tropsch synthesis [8,9]. In this case, the reduction of the mechanical resilience becomes an advantage, allowing the fibrous behavior to be lost and fine particles and powder flowability to be obtained with a reduced grinding energy [10]. In this case, the optimal treatment can be tuned according to the global mass loss due to thermal degradation [11]. However, it is very difficult to obtain this ideal treatment between and among particles, which emphasizes the need for predictive modeling tools.

Over the last few decades, numerous works have been devoted to the modeling of coupled heat and mass transfer in porous media: formulation, characterization, computational solution, and validation [12]. However, the specific domain of biomass torrefaction involves reactive transfer because chemical reactions occur together with heat and mass transfer. The thermo-activated nature of the chemical reactions together with the presence of reaction heats explains why this coupling is two-way: the reaction kinetics depend on the local value of temperature whereas the temperature field is influenced by the sink/source terms due to the reaction

---

[*] Corresponding author. Tel.: +33 141 131 679; fax: +33 141 131 437.
E-mail address: patrick.perre@ecp.fr (P. Perré).

0017-9310/$ - see front matter © 2013 Elsevier Ltd. All rights reserved.
http://dx.doi.org/10.1016/j.ijheatmasstransfer.2013.03.066

Nomenclature

C_p	specific heat (J kg^{-1} K^{-1})
c	molar concentration (mol m^{-3})
D_{AB}	diffusion coefficient of vapour in air (m^2 s^{-1})
ΔY_k	length of the control volume kin the longitudinal direction of the board (m)
ΔZ_k	height of the control volume kin the thickness direction of the board (m)
h	external heat transfer coefficient (W m^{-2} K^{-1})
h_m	external mass transfer coefficient (m s^{-1})
j	mass flux exchanged between the boards and the airflow (kg s^{-1} m^{-2})
q	mass flux in channels formed by two adjacent board layers (kg s^{-1} m^{-2})
L	characteristic length (m)
M_v	the molar mass of vapor (kg mol^{-1})
Nu	Nusselt number
Pr	Prandtl number
Re	Reynolds number
Sc	Schmidt number
Sh	Sherwood number
T	temperature (K)
x_v	molar fraction of vapor
x	airflow direction (m)

Superscripts and Subscripts:

a	air
b	bound
end	end board face
j	general index for a board layer
k	number of the CV on the board face
lo	lower board face
Ncv	total number of CVs on the board face
$surf$	surface
up	upper board face
v	vapour
∞	external value

heat. The complete modeling of these phenomena, at the particle level or at the level of a particle set, either for a fixed or agitated bed, is complex and was addressed here using a stepwise approach.

Most studies performed using a thermo-balance could be considered at the micro-particle level, a spatial size small enough for the time constant of the kinetic reactions to be larger than all time constants related to the heat and mass transfer inside the particles. This configuration is easy to obtain at low heating rates, but is more delicate to define at very large heating rates, such as those encountered in flash pyrolysis [13].

The literature available at the micro-particle level is much more abundant; see for example [14–17]. From the literature data, it becomes clear that multistage mechanisms are required for the model parameters to be valid over a certain range of temperature and/or heating rate values. In spite of the numerous papers devoted to this subject, one has to emphasize that most of the works, primarily based on the analyses of experimental data, are performed at linearly increasing temperature, with heating rates of some degrees per minute. This protocol prevents the slow reaction occurring at mild temperature levels to be accurately described.

At the macro-particle level, the primary variables (temperature, moisture content, degradation levels, internal pressure...) evolve in time and space. The variable fields must therefore be computed as the process evolves. This is the perfect scale at which reactive heat and mass transfers are to be accounted for. All models published in this field are more or less comprehensive, each one having its strengths and weaknesses. For research involving biomass pyrolysis, the strong point often lies in the reaction mechanisms and the volatiles production. This implies that the overpressure due to volatiles production and the induced gas velocities are usually taken into account [13,18–21]. Some of this research considers the change of physical properties and shrinkage from native wood to char. However, in most models, less attention is paid to moisture migration: either the particle is supposed to be fully dried before the process commences, or water evaporation is governed by a simplified expression. This is certainly due to the high temperature levels encountered during rapid pyrolysis, which causes the particle to dry very fast. A more recent work [22] proposed a comprehensive model able to account for most of the phenomena involved at the level of a macro-particle. For example, their model perfectly predicts the plateau at the boiling point of water when dealing with humid particles.

However, to our knowledge, none of these works focused their attention on the overshoot in temperature due to exothermic reactions. This phenomenon is very important in the domain of mild pyrolysis, where the temperature level is low (typically in the range 200–300 °C), but the residence time is very long (up to several hours). In such conditions, the effect of some tens of degrees might have a dramatic impact on the heterogeneity of the heat treatment. Based on our extensive knowledge in the field drying, we proposed a comprehensive model of heat and mass transfer able to deal with any MC field inside the product, including liquid water [23]. As a result of this feature, our model is perfectly able to produce the two pressure peaks measured during the heat treatment of a thick board: the first one being due to water evaporation and the second one due to volatiles production. In addition, by using both endothermic and exothermic reactions in the selected kinetics model, we were able to simulate the temperature overshoot observed in experimental data. Using this model, we proved that the presence of water delays the heat treatment phase and produces a more sudden temperature increase, which exacerbates the temperature overshoot. Notice that such an overshoot seems to be visible in the experimental data presented in [22] for a 44% moist wood log.

At the upper scale of a set of particles, either fixed or agitated, the published modeling work is rare. Di Blasi [24] modeled wood gasification in a 1-D fixed bed of particles. This model, which includes a drying zone and a pyrolysis zone, is able to capture the evolution of variables such as the solid and gas temperatures, molar fractions and reaction rates. Note that, as constant internal fields are assumed within each particle, this model is a single scale model.

Compared to this short literature review, the present work proposes a full dual-scale model, whereby each particle is accounted for at the upper scale. This gives rise to a full two-way coupling between the upper model (gas flow) and the particle level (macroscopic formulation). The kinetics model is supplied at each node of each particle model. Furthermore, the present work uses multistage mechanisms selected from different literature sources for each component of lignocellulosic components: cellulose, hemicelluloses and lignins [25]. Even though most literature data were obtained over a large range of temperature levels, the macroscopic model was adequately validated for mild pyrolysis [23]. The local model solves the set of equation in 2D, allowing for the effect of huge anisotropy of wood to be accounted for [26]. The dual-scale formulation adopted in this work follows the strategy proposed for the drying process [27,28]. Indeed, for what we believe is the first time, we propose a full dual-scale model of the heat treatment of wood (a stack of boards or a thick bed of particles), using a comprehensive 2-D formulation of reactive heat and mass transfers at the particle level, a configuration which is relevant at the industrial scale.

We first provide a brief overview of the dual scale model. Among the important features embedded in the comprehensive physical and chemical formulation at the particle model, emphasis should be given to (i) its ability to deal with any amount of moisture inside the product, including liquid water, (ii) its ability to consider water evaporation and production of volatiles on the internal pressure and (iii) its ability to predict the temperature overshoot due to exothermic reactions.

At the global scale, the two-way coupling between the boards and the channels formed by two adjacent board layers is considered throughout the process.

Thereafter, selected simulations are proposed to emphasize the effects of the initial moisture content and the board thickness on the heat treatment of boards. These effects are studied at both the board and stack scales. Thereafter several configurations are studied to limit the thermal run-away due to exothermic reactions within the board thickness and along the stack. Finally, following these test cases, an industrial treatment process is studied.

2. Dual-scale modelling of wood torrefaction

2.1. Modeling heat and mass transfer and thermal degradation at the local scale (the board)

At the local scale, the heat and mass transfer and the chemical modifications of the cell walls during the torrefaction period are taken into account in a multiphysics computational model known as *TransPore*. Indeed, during heat treatment, a two-way coupling exists between the heat and mass transfer (bound water, free water, vapor water, volatiles matters) and chemical mechanisms, including the thermal activation of the chemical reactions, together with the treatment of heat sources (or sinks) and the production of volatiles (Fig. 1a). The classical macroscopic formulation of heat and mass transfer phenomena that arise in hygroscopic porous media is presented in detail in [29]. The thermal decomposition of cellulose, hemicellulose and lignin components of the wood cell occurs via a series of chemical reactions [25]. The reaction rates are assumed to obey an Arrenhius law and each reaction has its own heat of reaction, either endothermic or exothermic. The temperature computed by *TransPore* for each control volume and at each discrete time level is used to obtain the reaction rates. Then, the resulting heats of reaction and gas production/consumption rate are computed by the pyrolysis model and integrated into the heat and mass balances computed by *TransPore*. This comprehensive model and its intricate two-way coupling, arising between the coupled heat and mass transfer and the degradation reactions, have been validated with experimental data [23].

Due to the huge permeability ratio between longitudinal and radial directions, the board length is of utmost importance in high temperature configurations [29]. We recently proved that the longitudinal migration also significantly affects the heat treatment [26]. Therefore, the 2D version of *TransPore* was chosen here at the particle level. In this work, only half the board length is computed, with symmetry boundary conditions applied on one side (see Fig. 1a). This computational domain is discretized by a set of 21 × 51 control volumes (CVs) for a 18 mm-thick board and 41 × 51 CVs for a 35 mm-thick board (radial and longitudinal directions). In the longitudinal direction, as the computed domain is 1 m long, the mesh is refined at the endpiece following a geometrical progression in such a way that the CVs have almost a square shape [30].

2.2. Modeling heat and mass transfer at the global scale (the stack)

The gas characteristics throughout the stack depend on the behavior of each single board and *vice versa*. A two-way coupling arises between the gas flow and the boards during the drying period [31] and also during the torrefaction period, where the heat produced by exothermic reactions occurring in each board can propagate over other boards situated downstream. In industrial plants, the gas flow is produced by the important pressure gap generated by fans placed upstream from the stack inlet. The gas flows in all tunnels formed between successive lumber layers by stickers placed along the flow every 50–70 cm. By construction, the gas flow through the stack is therefore simply a collection of mono-directional flows acting in parallel. This specific configuration allows the evolution of the gas characteristics (drying and heat treatment conditions throughout the board stack) to be captured using a simplified formulation. The energy and mass balances are written in each channels formed by two adjacent board layers (refer to Fig. 1b and c). In the case of heat treatment, volatiles produced by the chemical reactions are assumed to be perfectly mixed with the dry gas (N_2) of the gaseous phase assumed to form a homogeneous gas mixture [23]. In this way, the mass flux of this dry mixture, j_a exchanged between the boards and the airflow has to be taken into account in the heat and mass balances (see Eqs. (2) and (3)). C_{pa} in Eq. (3) is the specific heat at constant pressure of the dry mixture, which is assumed to be equal to the value of dry gas. In the following equations, each airflow channel is surrounded by upper board faces (superscript *up* of board layer *j*) and by lower board faces (superscript *lo* of board layer *j + 1*).

Moisture balance

$$\frac{dq_v}{dx} = j_v^{up,j} + j_v^{lo,j+1} \tag{1}$$

Balance of dry mixture

$$\frac{dq_a}{dx} = j_a^{up,j} + j_a^{lo,j+1} \tag{2}$$

Enthalpy balance

$$\begin{aligned}(C_{pa}q_a + C_{pv}q_v)\frac{dT}{dx} = {} & j_c^{up,j} + j_c^{lo,j+1} + j_v^{up,j}(C_{pv}(T_{surf}^{up,j} - T) \\ & + j_v^{lo,j+1}(C_{pv}(T_{surf}^{lo,j+1} - T) + j_a^{lo,j+1}(C_{pa}(T_{surf}^{lo,j+1} - T) \\ & + j_a^{up,j}(C_{pa}(T_{surf}^{up,j} - T)\end{aligned} \tag{3}$$

Note that the binary diffusion in the airflow is neglected due to the high value of the Peclet number. In the conservation Eqs. (1)–(3), the heat flux (j_c), the mass flux of vapor water (j_v) and the mass flux of dry mixture (j_a) are provided by the solution of each particle (via computation using one module of *TransPore* for each particle). In return, the solution of Eqs. (1)–(3), allows the partial vapor pressure and temperature of the airflow to be computed throughout the whole stack and to be used thereafter as boundary conditions in each module of *TransPore*. In this work, the mass flux of water vapor and dry mixture coming out of each board face are obtained as a weighted average over the CV faces of that board, including half the flux at the end piece. For example, the flux at the upper face of the board layer *j* is obtained using the following formula:

$$j_v^{up,j} = \frac{\sum_{k=1}^{Ncv\_up} j_{v,k}^{up,j}\Delta y_k + \sum_{k=1}^{Ncv\_end} \frac{j_{v,k}^{end,j}}{2}\Delta z_k}{\sum_{k=1}^{Ncv\_up}\Delta y_k} \tag{4}$$

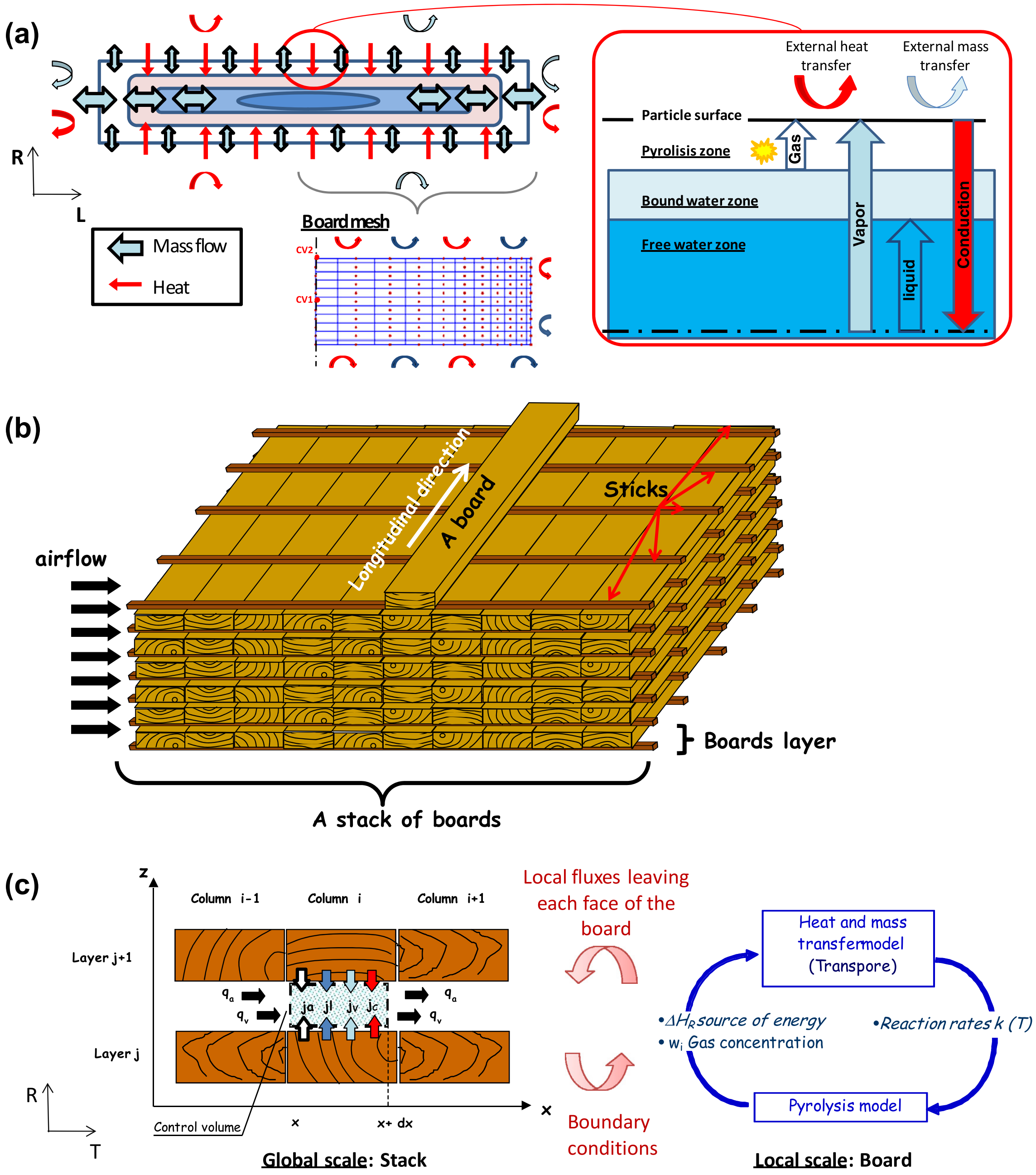

Fig. 1. Overview of the simulation strategy (a) multiphysics phenomena occurring at the particle scale at the beginning of the thermal treatment, (b) simplified schematic of the stack of boards with relevant terminology, (c) intrinsic coupled phenomena occurring between the stack and the board scales.

The usual boundary layer theory is used to estimate the external heat and mass transfer between the surface of the boards and the gas flow. The fluxes of total moisture and total enthalpy at the boundary respectively are of the following form:

$$j_v = h_m c M_v \ln\left(\frac{1-x_\infty}{1-x_b}\right)$$
$$j_c = h(T_b - T_\infty) \tag{5}$$

The gas flow channel between two adjacent board layers can be viewed as flow between parallel plates. The heat transfer coefficient is calculated from the Dittus-Boelter equation [32]:

$$Nu = 0.0230 Re^{4/5} Pr^{1/3} \tag{6}$$

where Nu is the Nusselt number, Re the Reynolds number and Pr the Prandtl number. The characteristic length L used to estimate the Nusselt and Reynolds numbers is equal to the hydraulic diameter, defined as four times the cross section area divided by the wetted perimeter, and taken as twice the sticker thickness in our configuration.

Eq. (6) is considered valid for turbulent flow ($Re > 10{,}000$). Indeed, the gas flow inside an industrial plant is highly turbulent, due to the presence of fans, the surface roughness of sawn boards and the geometrical defaults between successive boards. Consequently, Salin [33] suggested that Eq. (6) can be used with acceptable accuracy for lower values of Re. This turbulent regime also explains why constant transfer coefficients can be used throughout the stack.

The rectangular duct between two board layers and two stickers has a large dimensional ratio (more than 50). Thus, in this configuration, the hydraulic diameter can be estimated at twice the

Table 1
External heat and mass transfer coefficients calculated according to the airflow velocity for 2 cm thick stickers.

Gas velocity (m/s)	2	5	8	11
h (W m^{-2} °C^{-1})	14	29	42	55
h_m (m s^{-1})	0.014	0.028	0.041	0.054

sticker thickness. The airflow velocity and the external heat and mass transfer coefficients are assumed constant along the air flow path and across the duct section. The external mass transfer coefficient is calculated using the analogy between heat and mass transfer:

$$h_m = D_{AB}Sh/L \tag{7}$$

$$Sh = Nu \cdot Sc^{1/3}Pr^{1/3} \tag{8}$$

Table 1 depicts the estimated external transfer coefficient for a 2 cm thick sticker and according to the different airflow velocity along the stack. Additionally, Table 2 depicts the estimated external transfer coefficient for a 2 m/s airflow velocity for different sticker thicknesses.

2.3. The test configuration

As product parameters such as thickness and initial moisture content dramatically affect the homogeneity of the final product, 3 types of beech boards are simulated in the following section:

- **Case-study A:** a reference particle (3% MC, 35 mm thick) with parameter values as specified in Table 3.
- **Case-study B:** Higher moisture content (20% MC, 35 mm thick).
- **Case-study C:** Higher moisture content with a thinner board (20% MC, 18 mm thick).

For each case study, a full layer of boards has been computed to analyze the effect of the stack. The stack is composed of 11 boards arranged in layers (thus, 2.2 m deep along the air flow). The stack configuration is summarized in Table 4. In order to focus our attention on the stack effect rather than the heterogeneity of the initial product, all simulations were performed with identical boards in the present work. This allowed us to limit the stack calculations to one single stack layer.

The following schedule is applied as the heat-treatment procedure:

- Heating up to 110 °C at a rate of 2 °C/min, followed by a 5-h plateau (drying phase),
- Heating up to 220 °C at a rate of 1.5 °C/min, followed by a 5-h plateau
- Cooling down to 90 °C at a rate of −1.5 °C/min.

Using a personal computer with a 2.93 GHz i7 Intel processor, the CPU time is about 3 min for one single board simulation (Case-study A) and rises to about 40 min for a full board layer simulation.

Table 2
External heat and mass transfer coefficients calculated at 2 m s^{-} for different sticker thicknesses.

Sticker thickness (cm)	2	5	8	11
h (W m^{-2} °C^{-1})	14	12	11	10
h_m (m s^{-1})	0.014	0.011	0.010	0.010

Table 3
Input values used in the code *TransPore* for the reference board (A).

	Value	Unit
Thickness × Length	3.5 × 200	cm
Initial temperature	20	°C
Initial moisture content	3	%
Basal density	580	
Cellulose content	50	%
Hemicellulose content	25	%
Lignin content	25	%
Gaseous permeability in radial direction	4. 10^{-16}	m^2
Gaseous permeability in longitudinal direction	1.4. 10^{-12}	m^2
Diffusion resistance in radial direction	2. 10^{-3}	(−)
Diffusion resistance in longitudinal direction	1. 10^{-2}	(−)
External mass transfer coefficient	14. 10^{-3}	m s^{-1}
External heat transfer coefficient	14	W m^{-2} °C^{-1}

Table 4
Input values for the reference stack of boards used at the global scale.

	Value	Unit
Board dimensions (width × length)	200 × 2000	cm
Number of boards	11	(−)
Gas velocity	2	m s^{-1}
Sticker thickness	2	cm

3. Results and discussion

3.1. Coupled mechanisms arising due to the dual-scale (case study A)

Our first comment will be focused on case study A, the thick board (35 mm) with almost no initial moisture content (3% MC). Fig. 2 depicts the evolution of the temperature at surface and core (half-length) and the dimensionless pressure at the core for boards 1, 6 and 11, respectively situated at the stack inlet, in the middle and at the stack outlet.

Due to the one-way interaction along the gas flow, the first board is simply submitted to the process conditions set by the above-defined schedule and is not influenced by the presence of the stack. At first, we comment on the results obtained for this inlet board to provide a good understanding of the coupled mechanisms arising at the particle level, before advancing further towards the stack effect. A classical convection/conduction temperature profile is observed during the first temperature increase (up to the drying plateau at 110 °C). The surface temperature increases at first, as a result of the heat supplied by the gas flow by convective exchange and the core temperature follows this rise with a time delay due to conductive heat transfer. This transient period lasts for around 2 h and the temperature field is almost perfectly equilibrated at 110 °C after 3 h.

A second transient period appears at the end of the drying plateau, when the gas temperature rises up to the heat treatment plateau. As before, a temperature difference develops between the gas, surface and core temperatures, as a result of the resistances to heat transfer placed in series (convective transfer in the boundary layer and conductive transfer inside the product). Then, when the temperature overpasses 200 °C, one can see the core temperature increasing more quickly than the surface temperature, and eventually overtaking it. This is obviously the effect of exothermic reactions, triggered by the temperature level, which produces an internal source term. A temperature overshoot is observed, during which the convection/conduction mechanism act in the opposite way, the core being warmer than the surface and the external heat exchange coefficient operating to cool down the product. A maximum core temperature of 240 °C is observed for the inlet board after 3 h at the 220 °C-plateau.

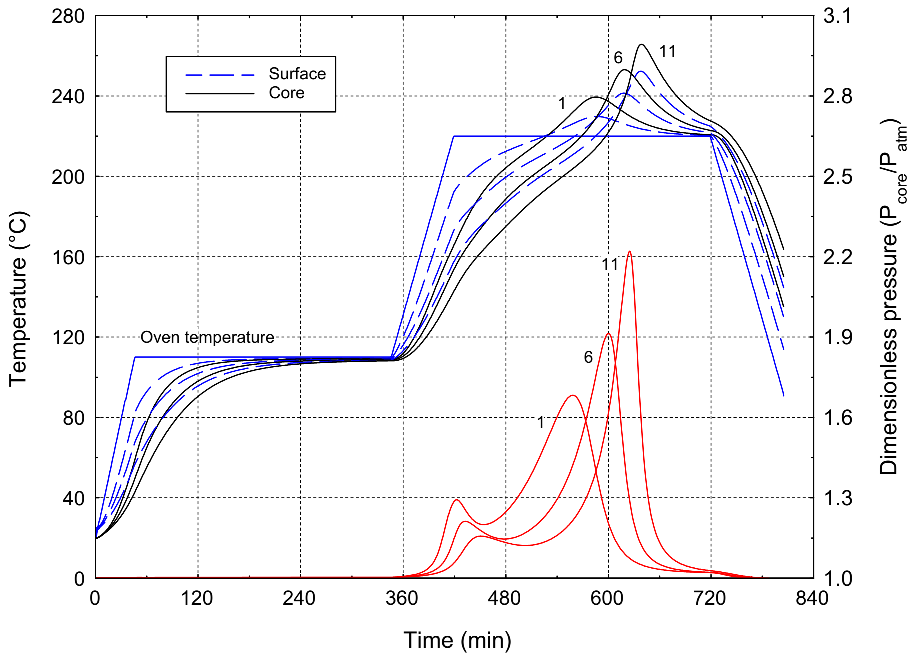

Fig. 2. Evolution of temperature (surface and core) and dimensionless pressure (core) for boards 1, 6 and 11 (from inlet to outlet). Case study A (MC = 3%, Thickness = 35 mm).

The double pressure peak is always very informative regarding the sequential occurrence and intensity of drying and heat-treatment. The first gas overpressure is due to water vaporization inside the product when the temperature significantly increases above the boiling point of water and the second peak appears due to the volatiles produced by the decomposition reactions [23]. In case study A, the first peak is weak because the initial MC is low. The second pressure peak reaches 1.7 bar for the first board.

Generally speaking, when the gas flow has to supply heat to the board, the gas flow temperature decreases along the stack and, progressively, the gas flow losses its ability to supply heat. On the contrary, when the boards supply energy to the airflow due to the exothermic reactions, the gas temperature increases along the stack and its ability to cool down the product worsens. In addition, the increased gas temperature is able to further activate the degradation reactions. The same trend holds for moisture exchange. For example, during the drying phase, the dew point increases along the stack due to the vapor flux exiting the boards. Together with the temperature drop, this effect further decreases the drying capacity of the gas flow. To summarize, the stack effect amplifies the trends observed for one single board. The interest of our dual-scale model lies in its potential to quantify these accumulative effects.

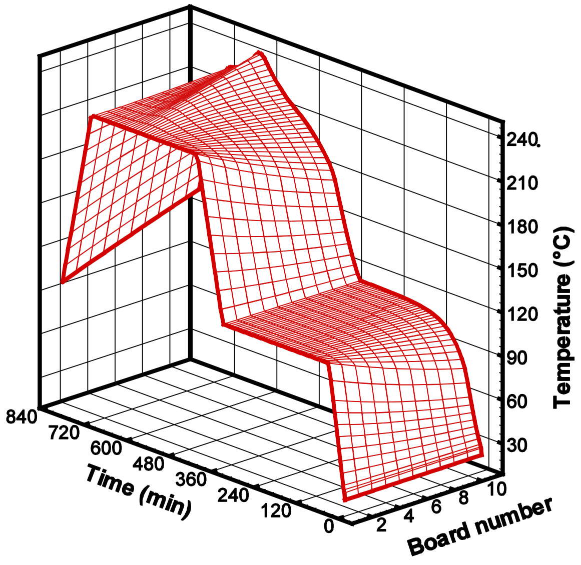

Fig. 3. Evolution of the gas flow temperature throughout the stack (case study A).

The initial heating up period perfectly confirms the above-mentioned trend: the time delay between the gas flow temperature evolution and the surface and the core temperatures of the board increases along the stack: 4 h (increasing period + plateau) is required for board 11 to approach the dry bulb temperature, compared to 2 h for the inlet board.

The evolution in time of the gas temperature profile along the stack (Fig. 3) perfectly depicts the existence of phases during which the gas temperature decreases from inlet to outlet (typically the two heating up periods) and phases with the opposite effect (the period of intense chemical degradation and the cooling down period). At the end of the drying plateau, the gas temperature profile is flat, which denotes a period without any exchange between the gas flow and the boards (one has to recall that Fig. 3 is plotted for case study A, which has almost no moisture to be removed).

The delay in the heat treatment of the outlet board (*n*°11) in comparison with the inlet board can be assessed by the second pressure peak, which occurs one hour later than for board 1 (Fig. 2). The higher level of temperature at the stack outlet intensifies the magnitude of the temperature overshoot. A thermal runaway is evident for board 11, whose temperature attains 266 °C at its core and 252 °C at its surface and with a pressure peak at 2.23 bar. A detailed analysis of the temperature field inside the board tells us that the exothermic reactions are first triggered close to the endpiece, which heats up first due to the presence of orthogonal exchange faces (Fig. 4). The temperature overshoot thereafter spreads throughout the length, whatever the board position. Note that at the end of the process, when the dry bulb temperature of gas at the stack inlet is 90 °C, the internal temperature of the outlet board is still at 140 °C. The pressure curves of boards 1, 6 and 11 confirm along the stack: a slower drying, with wider and lower

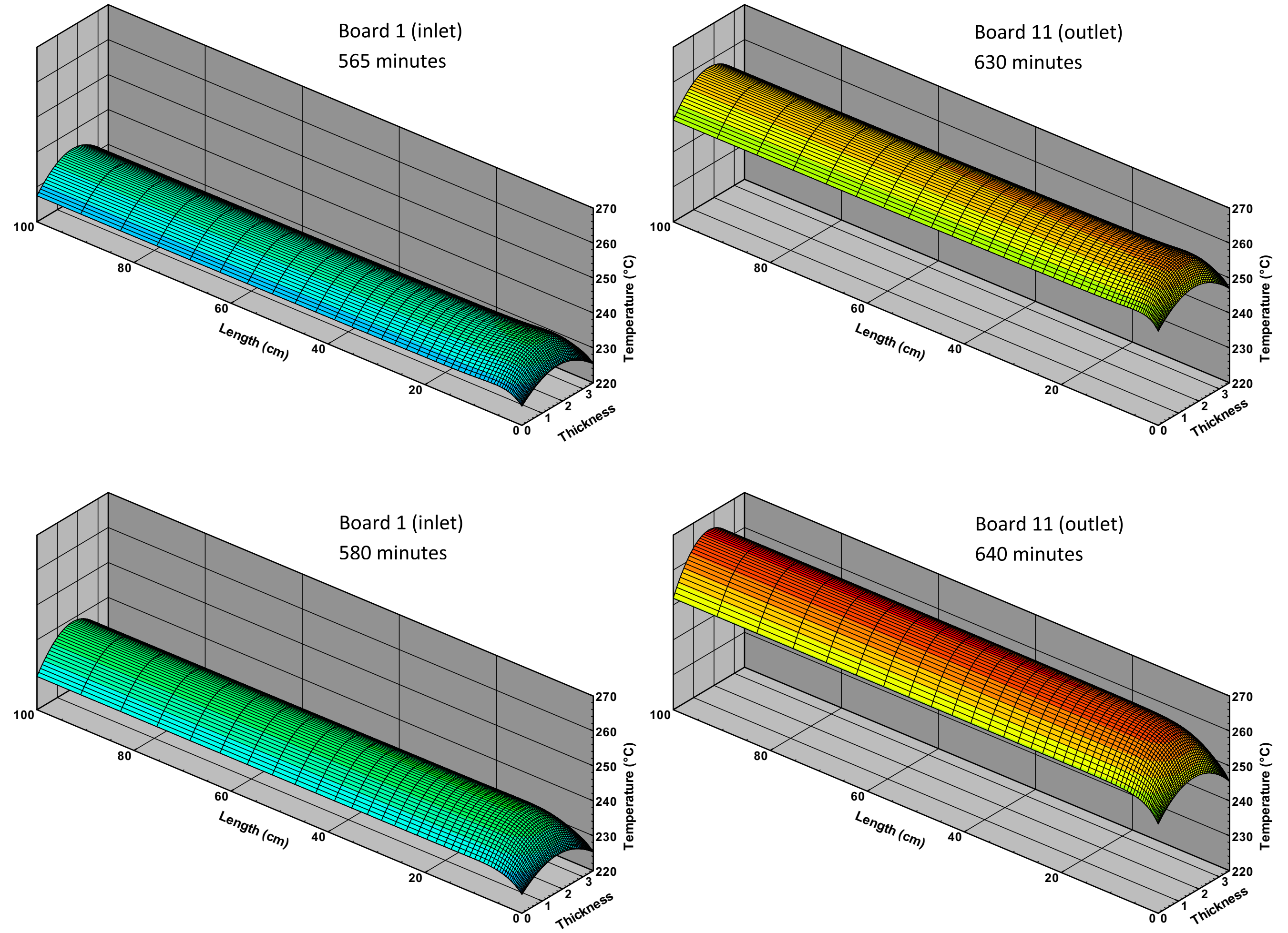

Fig. 4. Carpet plot of the temperature field inside board 1 (left) and board 11 (right), when the exothermic reactions start and depict a higher value near the endpiece (top) and when the core temperature reaches its maximum (bottom).

vaporization peaks and a treatment period becoming more intense, with sharper and higher volatiles peaks.

3.2. Effect of initial MC and thickness (case studies B and C)

Case study 2 (20% MC, 35 mm thick) allows the effect of initial moisture content to be analyzed (Fig. 5). Due to the high initial MC, the drying phase is far from complete at the end of the first plateau. This can be observed by the residual temperature between gas and surface at 360 min, even for board 1. This is required to supply, by convective transfer, the latent heat of evaporation needed to remove the moisture as water vapor. Consequently, a large part of evaporation takes place during the second heating-up period and even at the beginning of the heat treatment plateau. This delays the increase of the surface temperature, just because the convective heat exchange is used to supply the latent heat of evaporation, but delays even more the increase of the core temperature, which dries last. At this temperature level, drying occurs by internal vaporization which gives rise to an overpressure inside the product and a longitudinal water vapor migration in Darcy's regime due to the huge anisotropy ratio [29]. The massive and sudden evaporation occurring for board 1during the second heating-up period, and even during the beginning of the heat treatment plateau, gives rise to an important pressure peak (around 1.8 bar).An unexpected consequence of this drying behavior is that, once the drying of board 1 is completed, the temperature gradient inside the board is huge. Consequently, the core temperature increases rapidly towards the treatment temperature and triggers the exothermic reactions. Interestingly, this board, which requires a much higher amount of energy than case study A before the heat treatment presents a similar value of the maximum core temperature (240 °C). This maximum is however attained at 630 min against 580 min for case study A.

During the drying period, the decrease of dry-bulb temperature along the gas flow is larger than for case study A (22 °C at 120 min against 7 °C previously).The softer drying conditions imposed to boards 6 and 11induce a delay in the first gas pressure peak in comparison with board 1 (by about 65 min for board 11). Fig. 6 proves that board 1 still has a large amount of bound water at the beginning of the treatment plateau and is fully dried after one hour at this temperature level (480 min). With the stack effect, the MC extraction is even longer for the outlet board (n°11). At this position, drying hardly started at the end of the "drying" plateau and a significant amount of bound water still exists after one hour at the treatment plateau. Note the wider and lower pressure peaks obtained when the drying conditions softens, which is even more obvious than for case study A. Such conditions also induce a delay in the heat treatment of the outlet board in comparison with the inlet board, which can be assessed by the second pressure peak occurring 105 min later for board 11 with maximum temperature levels of 264 °C at the core and 244 °C at the surface. In this case, the temperature overshoot seems to be lower than for the case

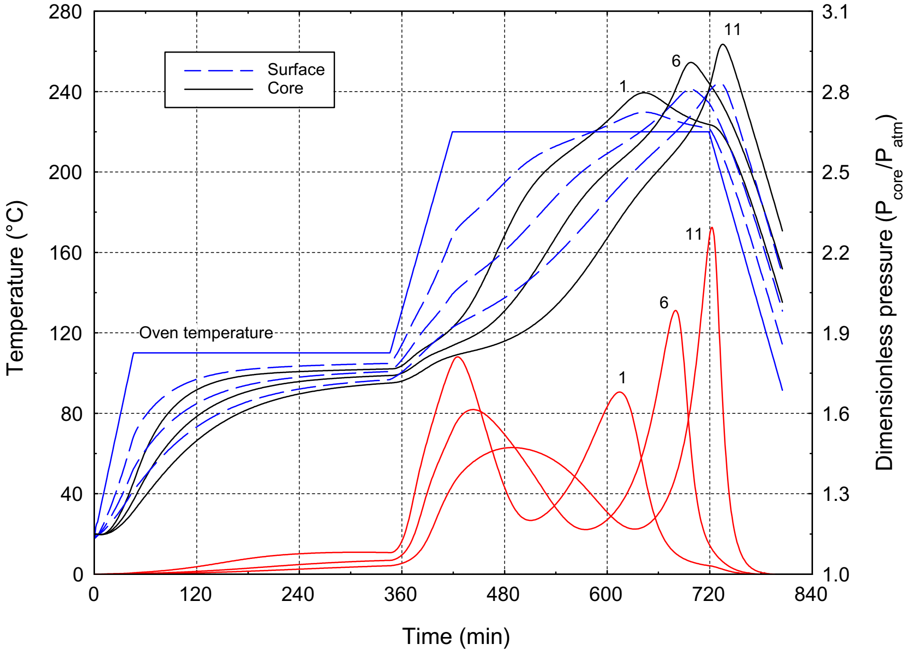

Fig. 5. Evolution of temperature (surface and core) and dimensionless pressure (core) for boards 1, 6 and 11 (from inlet to outlet). Case study B (MC = 20%, Thickness = 35 mm).

study A, but this is only because the time delay is so important that the treatment occurs when the gas flow already started to decrease, hence cooling down the board from its surface.

In the case of a thin board (case study C, Fig. 7), the time constants inside each board are reduced; typically by a factor 4 for all diffusive phenomena. In addition, as the water mass and the heat capacity are proportional to the thickness, the stack effect is typically reduced by a factor 2.This simple analysis is able to explain all the trends observed with 18-mm thick boards compared to 35-mm thick boards (case study B):

- The difference between the surface and core is now hardly visible, at least on the temperature values,
- The time between the two pressure peaks is significantly reduced;
- The cumulative effect of exothermic reactions is still significant, with a maximum temperature increasing from 227 °C for board 1 to 246 °C for board 11 and an overpressure peak from 1.28 to 1.50 bar.

Therefore, case study C tells us that, among all coupled mechanisms observed during this dual-scale configuration of wood torrefaction, the most difficult effect to reduce is the thermal run-away of the exothermic reactions due to the stack effect. This can be explained by the thermal activation of these reactions, which are therefore significantly faster as soon as the gas temperature increases due to the stack effect. In turn, this activation further increases the gas temperature for the next boards. This coupling is therefore likely to appear even for small particles, like those encountered in the use of lignocellulosic materials for energy purposes.

Fig. 8 depicts the density field of cellulose at the end of the thermal treatment process for different configurations, at the stack inlet and outlet. These graphs allow both the heterogeneity inside the particle and among particles to be quantified. In our example, the worse case for the outlet board is by far the reference configuration (A). The highest level of thermal degradation arose at the core of the outlet board, due to the cumulated effects of the macroscopic and global scales. Surprisingly, the treatment seems to be more homogeneous for the wet board (B): we just have to keep in mind that this effect is solely due to the important delay: for the outlet board, the heat treatment occurred at the end of the schedule and the product was already cooled down by the gas flow. This observation opens interesting possibilities for a control strategy able to produce a quite homogeneous treatment despite the large thickness. Finally, reducing the board thickness is very efficient in obtaining a homogeneous treatment, including within the worst board, the one situated at the stack outlet.

In summary, the behavior of each board of the stack results from coupled reactive transfer occurring inside each particle and between particles.

At the **local scale**, the heterogeneity of heat treatment observed within a single board results mainly from:

- the overheating of the board due to the exothermic reactions inside the product together with the insulation role of wood. The effect is significant for thick particles,
- the heterogeneity in initial moisture content. A higher initial MC delays the heat treatment that may therefore occur at different gas temperatures for a multistep treatment protocol.

At the **global scale**, the coupling between different boards along the gas flow amplifies the effect of heating or cooling of the product. Therefore, the transition from the first status (the gas flow heats up the product) to the second (the gas flow cools down the product) is more sudden in time and huge in amplitude. Degradation reactions are therefore triggered very rapidly and more intensely, as the gas temperature at the stack outlet can be higher than the set value (by almost 30 °C for our case study A). All together, this explains why the outlet board shifts very rapidly from a slow drying/heating phase to an intense treatment phase.

4. Reducing the cumulative effect of exothermic reactions

In order to exemplify the practical potential of this sophisticated dual-scale model, this section summarizes the effect of some process conditions on the computed temperature overshoots.

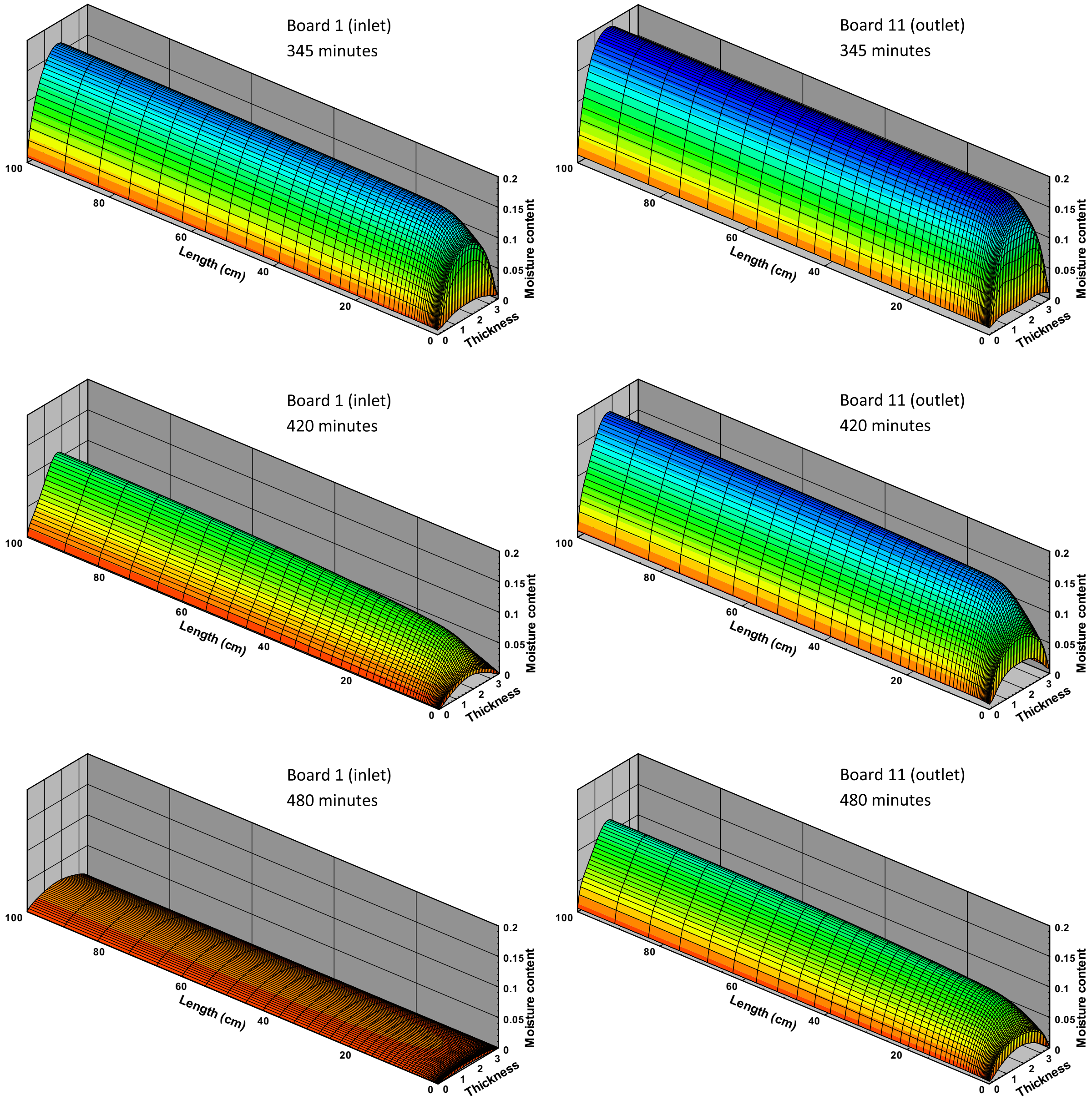

Fig. 6. Carpet plot of the moisture content field inside board 1 (left) and board 11 (right), at the end of the "drying" period (345 min), at the beginning of the treatment plateau (420 min) and after one hour of heat treatment (480 min).

Different strategies are studied for reducing the treatment heterogeneity:

- increasing the airflow velocity,
- increasing the sticker thickness,
- applying different periods of airflow reversal.

4.1. Increasing the airflow velocity

Increasing the airflow velocity is a standard approach taken to reduce the stack effect, by decreasing the variation in the variable fields along the stack. This must have a positive effect regarding the treatment homogeneity. On the other hand, a large airflow velocity increases the transfer coefficients (see Table 1), which tends to deepen the moisture and temperature profiles inside each board. A first observation is that this secondary effect works against the treatment homogeneity inside each particle.

In order to confirm these trends, three additional airflow velocities were computed in addition to the reference case study (A). Fig. 9 shows that by increasing the airflow velocity, the heterogeneity of treatment within and between the boards decreases. Indeed, the most important effect of increasing the gas velocity is to reduce the evolution of its properties along the stack.

Additionally, a higher velocity generates a lower external heat and mass resistance, which in turn increases the efficiency of the heat exchange between the airflow and the boards. The boards can be more easily cooled down by the exchange surfaces during the exothermic period and the thermal runaway can be avoided to a large extent. The difference between the maximum core and surface temperatures of each board is plotted in Fig. 9b. This information is interesting because it is strongly tied to the treatment heterogeneity inside that board. Its interpretation is subtler, as the value depicted for the inlet board seems to be independent of the airflow. Indeed, as the velocity increases, the transfer coefficients at the surface also increase, which would produce a deeper

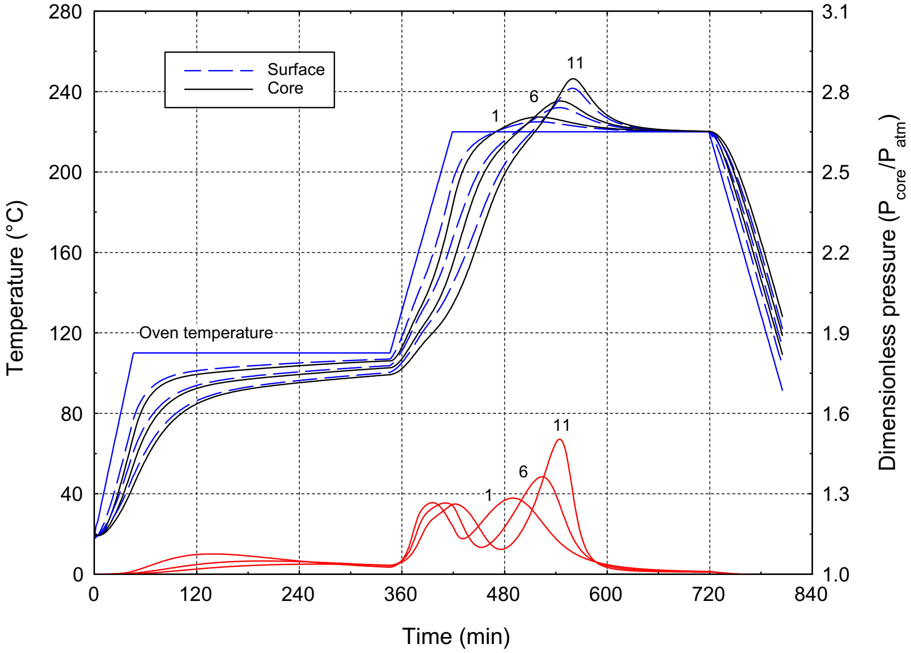

Fig. 7. Evolution of temperature (surface and core) and dimensionless pressure (core) for boards 1, 6 and 11 (from inlet to outlet). Case study C (MC = 20%, Thickness = 18 mm).

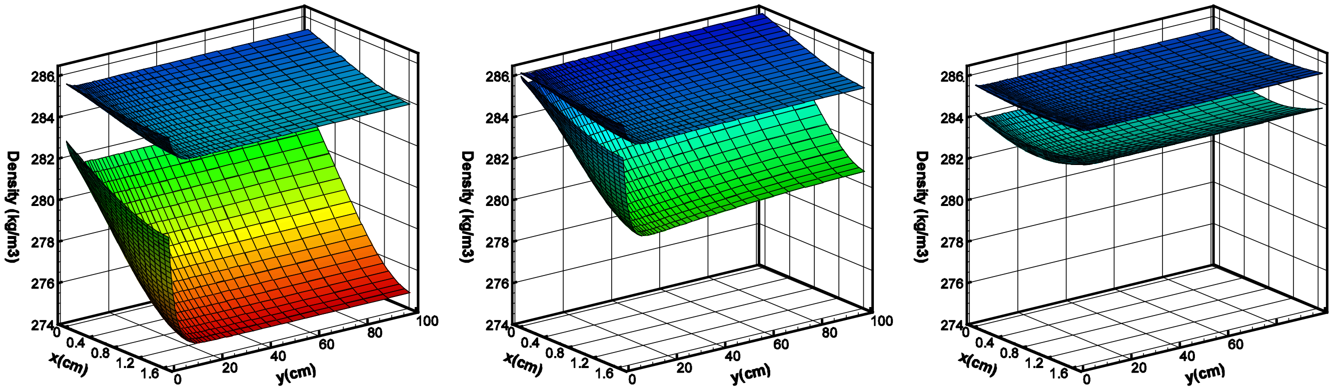

Fig. 8. Density fields of residual cellulose at the end of the thermal treatment for case study A (3% MC, 35 mm thick), case study B (20% MC, 35 mm thick) and for a thin board with low initial moisture content (3% MC, 18 mm thick). The top surface is for the inlet board (n°1) and the bottom one for the outlet board (n°11), where the cumulative effect of exothermic reactions produces a more severe degradation.

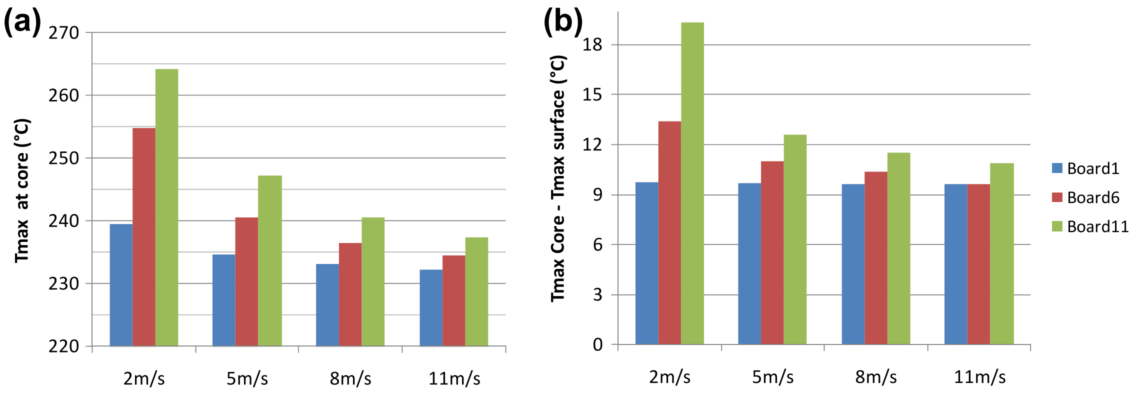

Fig. 9. Effect of gas flow velocity (a) maximal core temperature reached during the process by the 1st, 6th and 11th board from the inlet side for different *velocities*, (b) difference of maximal temperature between the core and surface of the same boards.

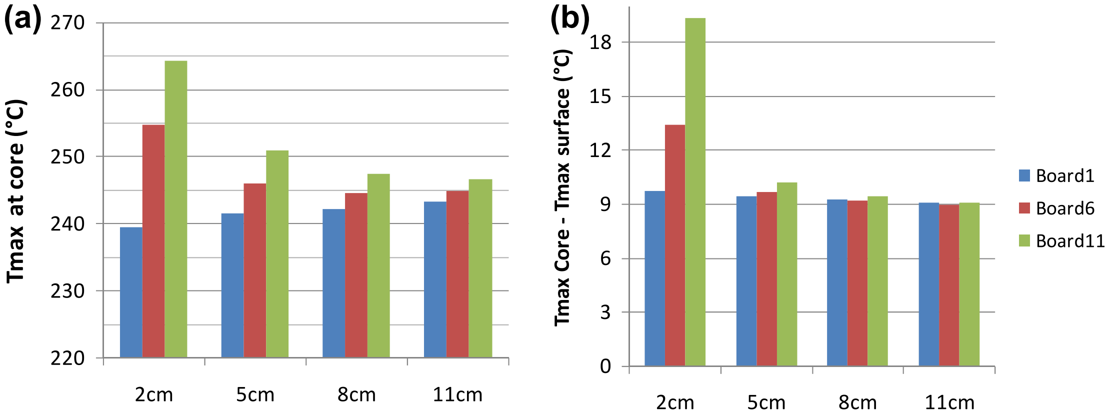

Fig. 10. Effect of sticker thickness: (a) Maximal core temperature reached during the process by the 1st, 6th and 11th board from the inlet side for different *thicknesses*, (b) difference of maximal temperature between the core and surface of the same boards.

temperature profile inside the board in the absence of an internal source term. However, during the exothermic period, the internal temperature profile is established to evacuate the heat source. If this heat source is almost the same, the temperature difference remains identical. In this case, a larger external heat transfer coefficient will simply reduce the temperature values by a constant amount. The maximum temperature will therefore be reduced at larger velocities, which is confirmed by Fig. 9a.

4.2. Increasing the sticker thickness

Increasing the sticker thickness is another solution to decrease the stack effect. Here, we increased the sticker thickness by the same amount as the gas flow mentioned in the previous paragraph. However, by reducing the stack effect, we now also reduce the transfer coefficients between the gas flow and each board (see Table 2). Lower external heat transfer coefficients reduce the thermal coupling between the gas flow and the boards, therefore reducing the potential to cool down the exchange surfaces during the exothermic period. As a result, increasing the sticker thickness is less efficient at increasing the velocity to limit the thermal run-away (Fig. 10a, to be compared to Fig. 9a). In spite of this loss of efficiency, lower transfer coefficients tend to decrease the temperature gradients inside each board. The temperature difference between the core and surface is then slightly lower in comparison with the strategy that increases the airflow velocity (Fig. 10b, to be compared to Fig. 9b).

4.3. Airflow reversal with different period of inversion

In conventional drying it is well known that the airflow reversal is a simple means to reduce the stack effect. This principle is therefore likely to apply for the heat treatment. In this section, we computed a series of simulations in which the gas flow is inverted at different periods of time (no reversal, every hour, every 25 min, every 5 min, and every minute). Fig. 11 summarizes the computed results in terms of the maximum temperature attained for three chosen boards (1 = inlet, 6 = middle and 11 = outlet) and the maximum difference between their core and surface temperatures.

As expected, the gas flow reversal systematically has a positive effect on the outlet board, the worst situation regarding the stack effect. However, the price to pay for this improvement is an increase of the treatment heterogeneity for the inlet board. The middle board seems to always slightly benefit from gas flow reversal. The effect of the reversal period is not so obvious to analyze. Indeed, for very short periods of time, the averaging effect over the stack is uniform: when the gas flow is inverted every 5 min, inlet and outlet boards become similar as their situation tends to be perfectly symmetrical. The middle board is the best in terms of temperature overshoot, as it never undergoes the full accumulative effect of exothermic reactions along the stack. For larger reversal

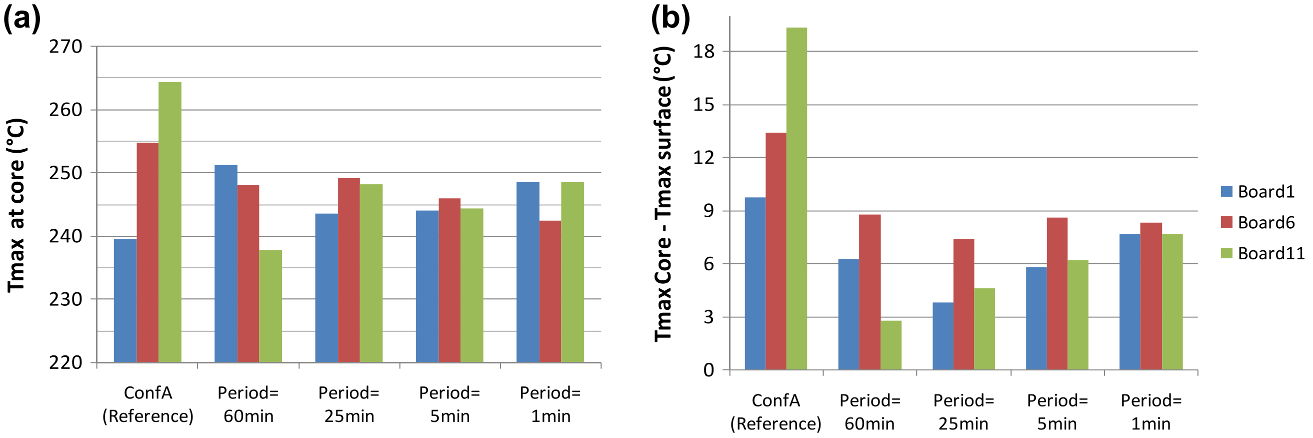

Fig. 11. Effect of gas flow reversal: (a) maximal core temperature reached during the process by the 1st, 6th and 11th board from the inlet side for different *reversal periods*, (b) difference of maximal temperature between the core and surface of the same boards.

periods, the symmetry is broken, as the history of each single board strongly depends on the sense of the gas flow when the risk of thermal run-away is maximal. This explains for example why a one-hour period is not beneficial for the inlet board. In this case, the period of intense exothermic reaction throughout the stack occurred while the gas flow was inverted.

In conclusion, the dual-scale model confirms that the gas flow reversal is a good way to reduce the heterogeneity due to the stack effect, and tells us that, in order to efficiently reduce the treatment heterogeneity, a short period of airflow reversal has to be chosen, typically 10 min or less.

5. Conclusion

A dual-scale computational model of the drying and heat treatment of wood was developed and used to study industrial configurations. At the local scale, the computational code solves the coupled heat and mass transfer and the thermal degradation mechanisms of the wood components. Among the important features of this particle model, emphasis should be given to (i) its ability to deal with any amount of moisture inside the product, including liquid water, (ii) its ability to consider water evaporation and production of volatiles on the internal pressure and (iii) its ability to predict the temperature overshoot due to exothermic reactions. At the global scale, the two-way coupling between the boards and the channels formed by two adjacent board layers is considered throughout the process.

The exothermic reactions occurring in each single board can propagate along the stack and pose a serious risk of thermal runaway. In our reference configuration, the maximum temperature reached at the core of the board increases from 239 °C (inlet board), to 264 °C (outlet board). A combination of a high gas flow velocity together with an inversion of the flow over a short period of time is a good way to dramatically reduce the stack effect.

We believe that based on its predictive ability, this sophisticated model has great potential, either for improving existing situations or in testing innovative process control, such as using a non-constant treatment temperature, which is the most likely way to reduce the heterogeneity in treating thick boards. We also intend to apply this model to the torrefaction process of a thick bed of particles, a configuration of particular interest for the use of lignocellulosic products as source of energy.

Acknowledgement

The authors wish to thank the anonymous reviewers for their insightful comments that improved the final presentation of this paper.

Appendix A. Supplementary data

Supplementary data associated with this article can be found, in the online version, at http://dx.doi.org/10.1016/j.ijheatmasstransfer.2013.03.066.

References

[1] J. Bourgeois, R. Guyonnet, Characterisation and analysis of torrefied wood, Wood Sci. Technol. 22 (1988) 143–155.
[2] P. Viitaniemi, Decay-resistant wood created in a heating process, in: VTT's communications. Espoo, 1997, pp. 22–23.
[3] M. Hakkou, M. Petrissans, P. Gerardin, A. Zoulalian, Investigations of the reasons for fungal durability of heat treated beech wood, Polym. Degrad. Stab. 91 (2006) 393–397.
[4] G. Almeida, J. Brito, P. Perré, Changes in wood-water relationship due to heat treatment assessed on micro-samples of three Eucalyptus species, Holzforschung 63 (2009) 80–88.
[5] S. Yildiz, E.D. Gezer, U.C. Yildiz, Mechanical and chemical behavior of spruce wood modified by heat, Build. Environ. 41 (2006) 1762–1766.
[6] G. Gündüz, S. Korkut, D.S. Korkut, The effects of heat treatment on physical and technological properties and surface roughness of Camiyani Black Pine (*Pinusnigra*Arn. subsp. pallasiana var. pallasiana) wood, Bioresour. Technol. 99 (2008) 2275–2280.
[7] Y. Xie, Y.X. Liu, Y.X. Sun, Heat-treated wood and its development in Europe, J. For. Res. 13 (2002) 224–230.
[8] G.M. Simmons, M. Gentry, Particle size limitations due to heat transfer in determining pyrolysis kinetics of biomass, J. Anal. Appl. Pyrolysis 10 (1986) 117–127.
[9] L. Wei, S. Xu, L. Zhang, H. Zhang, C. Liu, H. Zhu, S. Liu, Characteristics of fast pyrolysis of biomass in a free fall reactor, Fuel Process. Technol. 87 (2006) 863–871.
[10] P.C.A. Bergman, A.R. Boersma, J.H.A. Kiel, M.J. Prins, K.J. Ptasinski, F.J.J.G. Janssen, Torrefaction for entrained-flow gasification of biomass, Report ECN-C-05–067, The Netherlands, 2005.
[11] G. Almeida, J.O. Brito, P. Perré, Alterations in energy properties of eucalyptus wood and bark subjected to torrefaction: the potential of mass loss as a synthetic indicator, Bioresour. Technol. 101 (2010) 9778–9784.
[12] P. Perré, I.W. Turner, R. Rémond, Comprehensive drying models based on volume-averaging: background, application and perspective, in: Modern Drying Technology, Volume 1: Computational Tools at Different Scales, New York, Wiley, 2007, pp. 1–55.
[13] A.M.C. Janse, R.W.J. Westerhout, W. Prins, Modelling of flash pyrolysis of a single wood particle, Chem. Eng. Process. Process Intensif. 39 (2000) 239–252.
[14] G. Varhegyi, M.J. Antal, E. Jakab, P. Szabo, Kinetic modeling of biomass pyrolysis, J. Anal. Appl. Pyrolysis 42 (1997) 73–87.
[15] C. Branca, C.D. Di Blasi, Kinetics of the isothermal degradation of wood in the temperature range 528–708 K, J. Anal. Appl. Pyrolysis 67 (2003) 207–219.
[16] M.J. Prins, K.J. Ptasinski, F.J.J.G. Janssen, Torrefaction of wood Part 1. Weight loss kinetics, J. Anal. Appl. Pyrolysis 77 (2006) 28–34.
[17] T. Faravelli, A. Frassoldati, G. Migliavacca, E. Ranzi, Detailed kinetic modeling of the thermal degradation of lignins, Biomass Bioenergy 34 (2010) 290–301.
[18] J. Larfeldt, B. Leckner, M. Melaaen, Modelling and measurements of the pyrolysis of large wood particles, Energy Fuels 79 (2000) 1637–1643.
[19] C. Di Blasi, Physico-chemical processes occurring inside a degrading two-dimensional anisotropic porous medium, Int. J. Heat Mass Transfer 41 (1998) 4139–4150.
[20] C. Di Blasi, Modeling chemical and physical processes of wood and biomass pyrolysis, Prog. Energy Combust. Sci. 34 (2008) 47–90.
[21] M. Gronli, M. Melaaen, Mathematical model for wood pyrolysis – comparison of experimental measurements with model predictions, Energy Fuels 14 (2000) 791–800.
[22] U. Sand, J. Sandberg, J. Larfeldt, R.B. Fdhila, Numerical prediction of the transport and pyrolysis in the interior and surrounding of dry and wet wood log, Appl. Energy 85 (2008) 1208–1224.
[23] I.W. Turner, P. Rousset, R. Rémond, P. Perré, An experimental and theoretical investigation of the thermal treatment of wood in the range 200–260°C, Int. J. Heat Mass Transfer 53 (2010) 715–725.
[24] C. Di Blasi, Modeling intra- and extra-particle processes of wood fast pyrolysis, AICHE J. 48 (2002) 2386–2397.
[25] P. Rousset, I.W. Turner, A. Donnot, P. Perré, Choix d'un modèle de pyrolyse ménagée du bois à l'échelle de la microparticule en vue de la modélisation macroscopique, Ann. Forest Sci. 63 (2006) 213–229.
[26] R. Rémond, I. Turner, P. Perré, Modelling the drying and heat treatment of lignocellulosic biomass: 2D effects due to the product anisotropy, Drying Technol. 28 (2010) 1013–1022.
[27] P. Perré, Multiscale aspects of heat and mass transfer during drying, Transp. Porous Media 66 (2007) 59–76.
[28] P. Perré, Multiscale modelling of drying as a powerful extension of the macroscopic approach: application to solid wood and biomass processing, Drying Technol. 28 (2010) 944–959.
[29] P. Perré, I. Turner, A 3D version of TransPore: a comprehensive heat and mass transfer computational model for simulating the drying of porous media, Int. J. Heat Mass Transfer 42 (1999) 4501–4521.
[30] P. Perré, A. Degiovanni, Simulation par volumes finis des transferts couplés en milieux poreux anisotropes: séchage du bois à basse et à haute température, Int. J. Heat Mass Transfer 33 (1990) 2463–2478.
[31] P. Perré, R. Rémond, A dual scale computational model of kiln wood drying including single board and stack level simulation, Drying Technol. J. 24 (2006) 1069–1074.
[32] P. Incropera, D.P. De Witt, Fundamentals of Heat and Mass Transfer, John Wiley and Sons, New York, 1985.
[33] J.G. Salin, Prediction of heat and mass transfer coefficients for individual board and boards surface, in: Proc. of the 5th International IUFRO Wood Drying Conference, Quebec, Canada, 1996, pp. 49–58.